A&A 504, 635–640 (2009)
DOI: 10.1051/0004-6361/200912409

Astronomy & Astrophysics

Dimethyl ether: laboratory spectra up to 2.1 THz

Torsion-rotational spectra within the vibrational ground state⋆

C. P. Endres[1], B. J. Drouin[2], J. C. Pearson[2], H. S. P. Müller[1], F. Lewen[1], S. Schlemmer[1], and T. F. Giesen[1]

[1] I. Physikalisches Institut, Universität zu Köln, Zülpicher Str. 77, 50937 Köln, Germany
e-mail: endres@ph1.uni-koeln.de
[2] Jet Propulsion Laboratory, California Institute of Technology, Pasadena, CA 91109-8099, USA

Received 30 April 2009 / Accepted 4 June 2009

ABSTRACT

Dimethyl ether (CH_3OCH_3) is one of the largest organic molecules detected in the interstellar medium. As an asymmetric top molecule with two methyl groups which undergo large amplitude motions and a dipole moment of μ = 1.3 D, it conveys a dense spectrum throughout the terahertz region and contributes to the spectral line confusion in astronomical observations at these frequencies. In this paper, we present rotational spectra of dimethyl ether in its ground vibrational states, which have been measured in the laboratory and analyzed covering frequencies up to 2.1 THz. The analysis is based on an effective Hamiltonian for a symmetric two-top rotor and includes experimental data published so far. Frequency predictions are presented up to 2.5 THz for astronomical applications with accuracies better than 1 MHz.

Key words. ISM: molecules – molecular data – methods: laboratory – techniques: spectroscopic – radio lines: ISM – submillimeter

1. Introduction

Dimethyl ether (DME) is one of the simplest molecules with two methyl groups undergoing large amplitude motions. The internal rotation of both methyl groups combined with a relatively large dipole moment of μ = 1.302 D causes a strong complex spectrum with a high spectral line density over the THz region.

As with other highly saturated molecules, it is found in high abundance in star-forming regions, such as the Orion nebula, at rotational temperatures of around 200 K (Schilke et al. 1997, 2001). Since the first interstellar detection by Snyder et al. (1974), more than 200 transitions have been assigned to DME in various interstellar spectra, which led to unambiguous identifications. The formation process of DME still remains unclear. Current gas-grain models assume that the surface reaction $CH_3 + CH_3O \rightarrow CH_3OCH_3$ is the most likely formation route in warm dense regions (Garrod & Herbst 2006). These models predict strong variations of the abundance during the evolutionary stage of the protostar (Garrod et al. 2008). Further studies on DME can therefore provide important constraints on the evolutionary cycle of large organic molecules and chemical pathways in these interstellar objects. The rich chemistry in these environments is reflected also in the complexity of astronomical spectra. The analysis of these spectra is mostly limited by line confusion rather than the background noise and strongly depends on the knowledge of accurate rest frequencies of the major species in this object. A significant fraction of the observed transitions belong to a limited number of often saturated molecules such as methanol, CH_3CH_2CN, CH_3CHO, CH_3COOH, CH_3CN, SO_2, and DME. Transitions of these molecules are distributed over the THz frequency region up to around 2 THz at temperatures of 150 K as shown in the stick spectrum of DME in its vibrational ground state (Fig. 1). The most intense transitions are found at 1 THz. Therefore a complete understanding of these few species is essential in overcoming line confusion for the detection of more exotic species.

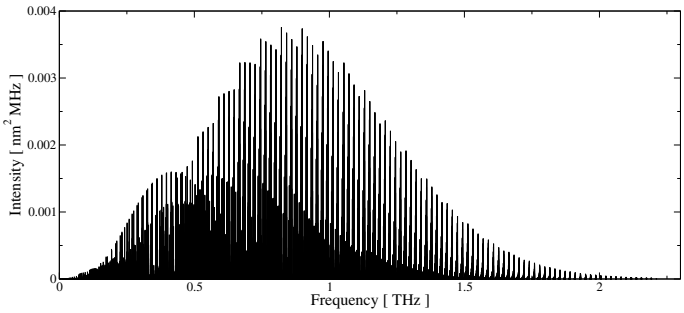

Fig. 1. Stick spectrum of dimethyl ether in its vibrational groundstate. The value of the intensity is calculated for 150 K. The most intense transitions are found at frequencies of around 950 GHz.

New observatories such as ALMA (Atacama Large Millimeter Array) and Herschel will provide access to the THz region with greatly improved sensitivity. Thus the need for accurate transition frequencies is substantially enhanced, especially in the THz range where reliable spectroscopic data are still relatively poor. In addition, pure rotational spectra within excited vibrational states must be investigated.

The pure rotation-torsional spectrum of DME in its vibrational ground state has been studied in the laboratory for more than 40 years. Major steps towards its understanding were the derivation of symmetry properties and nuclear spin statistics by Myers & Wilson (1960) and the determination of the structure and dipole moment by Blukis et al. (1963). By measuring a small number of microwave transitions, Durig et al. (1976) were

⋆ Table A.1 is only available in electronic form at the CDS via anonymous ftp to cdsarc.u-strasbg.fr (130.79.128.5) or via http://cdsweb.u-strasbg.fr/cgi-bin/qcat?J/A+A/504/635

able to determine the potential barrier height to internal rotation. The first predictions for astronomical purposes were published by Lovas et al. (1979) in their review of the vibrational ground state transitions. They also included new measurements, which were considerably extended by the work of Neustock et al. (1990). The most comprehensive experimental work so far on the rotational ground state spectra has been published by Groner et al. (1998). They measured and assigned another 1800 transitions and accessed frequencies up to 550 GHz and J quantum numbers up to 49. Their analysis was based on an effective Hamiltonian proposed by Groner (1997). The experimental dataset including all previously published rotational transition frequencies was reproduced within experimental uncertainties and accurate frequency predictions up to 600 GHz were calculated. Despite these extensive efforts, the quality of predicted rotational transition frequencies of DME for the THz region does not satisfy the needs of astronomers to model current astronomical spectra accurately. The objective of the present work is to improve the quality of predicted ground state rotational transition frequencies and to extend the dataset to frequencies above 2 THz. For this study, additional spectra were recorded and analyzed from 38 GHz up to 2.1 THz accessing J and K values up to 70 and 30, respectively. The assigned transitions have been modeled using the same effective Hamiltonian model as in Groner (1997) and frequency predictions up to 2.5 THz have been derived.

2. Theoretical model

DME is an asymmetric top molecule close to the prolate limit. Ray's asymmetry parameter is $\kappa = -0.9218$. The dipole moment ($\mu = 1.302$ D determined by Blukis et al. 1963) coincides with the axis of symmetry and a moderately strong b-type spectrum is observed. Weak c-type transitions, which are forbidden in first order approximations, also occur in the spectrum. The two methyl groups undergo large amplitude motions around the C-O bond. The symmetry is given by the molecular symmetry group G_{36}. In the vibrational and torsional ground state, the barrier to torsion is relatively high ($\approx$915 cm^{-1}) and the classification of the wavefunctions in terms of C_{2v} symmetry, which is the symmetry in the rigid rotor limit, is still useful. Each rotational level, which has a degeneracy of nine (3x3 periodic potential), splits into four substates AA, AE, EA, and EE, due to the nonzero tunneling probability. The labeling of the substates is given in the commonly used notation of the $C_{3v}^{-} \otimes C_{3v}^{+}$ group derived by Myers & Wilson (1960). Rotational transitions occur only within each substate. The splitting in the ground state is typically of the order of several megahertz, but the splitting between EA and AE is mostly unresolved in Doppler-limited measurements. The spin statistical weights were derived by Myers & Wilson (1960) as 6(AA), 16(EE), 2(AE), 4(EA) and 10(AA), 16(EE), 6(AE), 4(EA) for *ee-oo* and *eo-oe* rotational transitions, respectively. Thus a characteristic triplet is usually observed with the most intense transition (EE) located in-between two equally intense transitions (AE/EA and AA).

The analysis is based on an effective Hamiltonian proposed by Groner (1997), which is briefly summarized below. The Hamiltonian is derived using a Fourier expansion series of the potential, the rotational terms and the eigenfunctions in terms of the free rotor functions. The wavefunctions are expanded as a direct product of symmetric rotor functions $|JKM\rangle$ and internal motion basis functions $|v\sigma_1(K)\sigma_2(-K)\rangle$:

$$|JKMv\sigma_1\sigma_2\rangle = |JKM\rangle\,|v\sigma_1(K)\sigma_2(-K)\rangle\,. \tag{1}$$

The quantum number v distinguishes different vibrational states and σ_1, σ_2 are torsional symmetry numbers labeling the substates. In the case of DME each internal motion has a threefold periodicity ($n = 3$) and $0 \le \sigma_k \le 2$ ($k = 1, 2$). Each possible combination corresponds to one of the four substates. The nondegenerate level AA corresponds to $(\sigma_1\sigma_2) = (0, 0)$, the fourfold degenerate substate EE corresponds to the combinations $(1, 0)$, $(2, 0)$, $(0, 1)$, $(0, 2)$, and the two twofold degenerate substates AE, EA correspond to $(1, 1)$, $(2, 2)$ and $(1, 2)$, $(2, 1)$, respectively. It has been shown in Groner (1997) that the matrix elements of the Hamiltonian can be expressed in this basis set as

$$\langle JK'Mv\sigma_1\sigma_2|\,H\,|JKMv\sigma_1\sigma_2\rangle = \sum_{K_1}\sum_{K_2} Y_{K'K}(K_1, K_2)\Sigma_0 + \sum_l \langle JKM|R_l|JKM\rangle\,\Sigma_l. \tag{2}$$

The matrix $Y_{K'K}(K_1, K_2)$ is defined as

$$\begin{aligned} Y_{K'K}(K_1, K_2) = \frac{1}{2}\,(&\langle JK'M|JK_1M\rangle\,\langle JK_1M|JK_2M\rangle \\ &\times\langle JK_2M|JKM\rangle + \langle JK'M|JK_2M\rangle \\ &\times\langle JK_2M|JK_1M\rangle\,\langle JK_1M|JKM\rangle) \end{aligned} \tag{3}$$

and is composed of matrix elements $\langle JK_kM|JKM\rangle$. They arise from a projection of the molecule fixed reference axis system into an axis system whose z_k axis is parallel to the ρ axis of the k-th internal rotor. K_k is the quantum number of the projection of the overall angular momentum J onto the z_k axis. For DME $Y_{K'K}(K_1, K_2)$ only depends on the polar angles β_k of the vectors ρ_k with respect to the reference axes due to symmetry constraints with $\beta := \beta_1 = \pi - \beta_2$. The prefactors Σ_0 and Σ_l of the rotational operators which occur in Eq. (2) are the expectation values of torsional operators in the $|v\sigma_1(K)\sigma_2(-K)\rangle$ basis. They are two-dimensional Fourier series in $\sigma_1 - \rho K_1$ and $\sigma_2 - \rho K_2$ (or in $\sigma_1 - \rho K$ and $\sigma_2 + \rho K$) because the periodic property of the potential and kinetic energy terms causes a periodicity of the eigenfunctions of the torsional Hamiltonian. The Fourier series are given by

$$\Sigma_0 = \epsilon_{00} + 2\sum_{q>0}\left[C'_{qq}\epsilon_{qq} + C'_{q-q}\epsilon_{q-q}\sum_{q'=-q+1}^{q-1}(C'_{qq'} + C'_{q'q})\epsilon_{qq'}\right] \tag{4}$$

and

$$\begin{aligned} \Sigma_l = T_l^{(\kappa)}{}_{00} + 2\sum_{q>0}\Big[&C_{qq}T_l^{(\kappa)}{}_{qq} + C_{q-q}T_l^{(\kappa)}{}_{q-q} \\ &\cdot\sum_{q'=-q+1}^{q-1}(C_{qq'} + C_{q'q})T_l^{(\kappa)}{}_{qq'}\Big] \end{aligned} \tag{5}$$

with $\kappa = K - K'$ and

$$\begin{aligned} C'_{qq'} &= \cos\left(2\pi\left(q\left(\sigma_1 - \rho K_1\right) + q'\left(\sigma_2 - \rho K_2\right)\right)/n\right) \\ C_{qq'} &= \cos\left(\pi\left(q\left(2\sigma_1 - \rho\left(K + K'\right)\right)\right.\right. \\ &\quad \left.\left. + q'\left(2\sigma_2 + \rho\left(K + K'\right)\right)\right)/n\right). \end{aligned} \tag{6}$$

The coefficients $\epsilon_{qq'}$ and $T_l^{(\kappa)}{}_{qq'}$ in these series are actually the matrix elements of the torsional energy and of functions depending on both coordinates of internal roatation, respectively, in a basis of localized functions which can be obtained from the eigenfunctions of the torsional Hamitonian. These coefficents are the spectroscopic parameters together with the internal rotation parameter ρ and the polar angle β. Fourier coefficents with $q = q' = 0$ are equivalent to the rigid-rotor rotational parameters and only Fourier coefficients with $q > 0$ or $q' > 0$, so-called tunneling parameters, arise form the interaction between

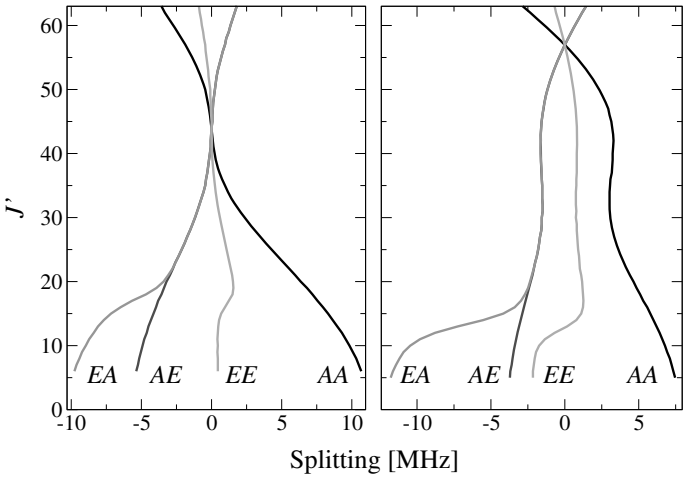

Fig. 2. Torsional splitting of energy levels with $K_c = J - K_a + 1$ in the vibrational ground state of DME. Levels having quantum numbers $K_a = 6$ are shown on the left, levels with $K_a = 5$ are shown on the right. The energy has been calculated neglecting all tunneling parameters. The splitting depicted in this figure is obtained by subtracting this value from the energy derived if all fitted parameters are included.

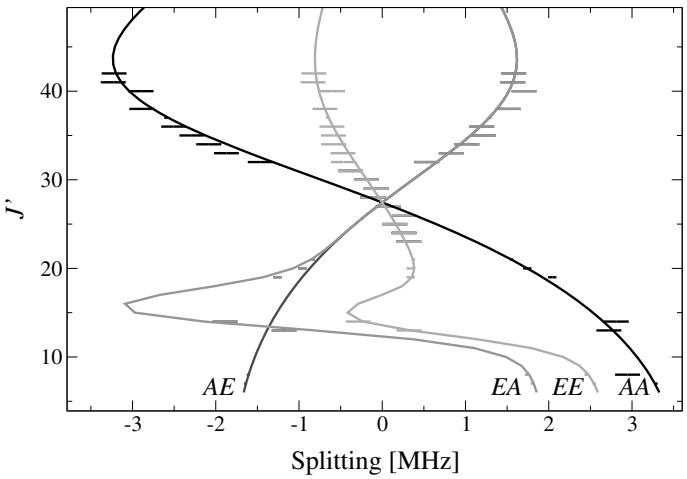

Fig. 3. Torsional splitting for Q-branch transitions with $K_a = 6-5$, and $K_c = J - K_a + 1$ in the vibrational ground state of DME. The splitting is calculated by subtracting the predicted transition frequency which neglects all tunneling parameters from the transition frequencies. The solid lines connect calculated frequencies belonging to one of the four substates. Experimental data is shown as errorbars.

internal and overall rotation. As has been shown before for the vibrational ground state of DME, the first order tunneling term of each series ($q = 1$, $q' = 0$) is usually sufficient for a rapid convergence of the fit.

Results of this model approach will be discussed in Sect. 4. To illustrate the effect of the tunneling on the energy diagram and the corresponding transition frequencies, one example is given in Figs. 2 and 3. Figure 2 shows the splitting of energy levels with quantum numbers $K_a = 6$ (left) and $K_a = 5$ (right), and $K_c = J - K_a + 1$ in the vibrational ground state of DME. In Fig. 3, Q-branch frequencies connecting lower states described in Fig. 2 (right panel) and upper states (left panel) are plotted together with experimentally determined values. This favorable comparison is a result of a rather limited set of tunneling parameters, which will be discussed in detail in the analysis section (Sect. 4).

3. Experimental details

Torsion-rotational spectra of DME were recorded in Cologne and at the Jet Propulsion Laboratory (JPL) in the millimeter and submillimeter wave regions. Several broad scans were performed, which cover several frequency regions completely. In Cologne, the complete frequency range from 38–56 GHz and from 550–610 GHz was recorded. Furthermore, numerous spectra of single transitions have been measured up to almost 2.1 THz. Below 60 GHz, a commercial synthesizer was used as a radiation source and the signal was detected after a 6 m absorption cell by a Schottky diode. Higher frequencies were accessed with several phase locked Backward Wave Oscillators (BWO) (see Lewen et al. 1998, for details). The high output power of the BWOs gave access to weaker transitions up to 900 GHz with good signal to noise ratios. The line survey from 550–610 GHz and transition frequencies above 900 GHz were carried out with BWOs in combination with superlattice frequency multipliers as the radiation source. For more technical details see Endres et al. (2007). Both setups used InSb hot electron bolometers for detection and an absorption cell of 3 m length. The BWOs were phase locked to a rubidium reference to assure a frequency stability of $\Delta f/f = 10^{-11}$. In Cologne, spectra were recorded with a $2f$-frequency modulation technique for better signal to noise ratios. At the JPL, frequency stabilized multiplier chains were applied to record broad band spectra from 766 to 930 GHz, 983 to 1158 GHz, and from 1.58 to 1.67 THz. The radiation was detected by a Si-composite bolometer after doubly passing the 2.5 m absorption cell. Tone burst modulation was used for detection. The JPL setup is locked to one part in 10^{12}. Thus, the accuracy depends only on the quality of the spectrum. A detailed description of this setup is given in Drouin et al. (2005). All measurements were carried out at room temperature and the pressure in the absorption cell was typically of the order of 1 Pa, but pressures up to 10 Pa have been used to measure weaker lines.

Lines were not included in the analysis if the line profile was not sufficiently well reproduced due to very complicated structure or due to unknown blends, because the uncertainty for those lines is easily underestimated. A significant number of line assignments was verified by calculating closed loops of transitions. The quality of predicted line position and the usually characteristic intensity patterns helped in assigning the transitions.

4. Observed spectrum and analysis

1602 new lines were measured in total and assigned to 4827 transitions. Energy levels including $J = 70$ and $K = 30$ were accessed. A summary of the experimental lines is given in Table 1. The line accuracies were estimated for each single line individually with regard to the line profile fit and are listed in the supplementary material. The accuracy typically was 100 kHz. For isolated single lines, accuracies of 20 kHz were achieved. Frequently, lines overlapped due to an unresolved splitting or by other nearby lines and the line profile was distorted. Although the blend of lines was considered in the line profile fit, it generally was the most significant contribution to the uncertainty of experimental line frequencies. In the frequency range from 39–56 GHz, 344 transitions were recorded, accessing energy levels with $J = 54$ and $K = 19$. The line widths are small enough at these frequencies to resolve the torsional splitting into the four substates AA, EE, AE, and EA completely for a large number of transitions and at most blending of the substates AE and EA was observed. A transition with completely resolved torsional splitting is shown in Fig. 4. The fundamental spin statistical weights

Table 1. Characterization of the different datasets used in the fit.

Source[a]	# of Transitions[b]	Max. J	Max K_a	Frequency [GHz]		σ
				Min.	Max.	
Synthesizer (Cologne)	344 (259)	54	19	39	56	1.02
BWO (Cologne)	586 (273)	70	27	69	897	0.90
BWO + SL (Cologne)	1663 (635)	63	27	263	2099	0.95
Multiplier chain (JPL)	2234 (435)	67	30	780	1665	1.08
Niide & Hayashi (2003)	16 (13)	7	2	12	25	1.77
Durig et al. (1976)	20 (15)	4	1	29	36	0.50
Lovas et al. (1979)	191 (157)	22	6	9	112	0.74
Neustock et al. (1990)	79 (66)	24	5	63	222	0.96
Groner et al. (1998) (Klystron)	962 (702)	25	6	94	544	1.08
Groner et al. (1998) (FASSST)	735 (386)	49	10	263	340	0.85

[a] The first four rows summarize transitions measured within this work.
[b] The number of assigned transitions is given followed by the number of different frequencies in parentheses. The last column shows the unitless standard deviation of the dataset in the fit.

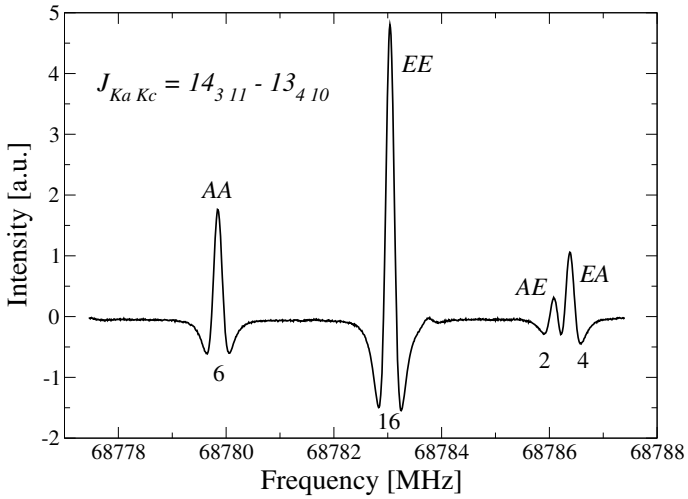

Fig. 4. Rotational transition ($J_{K_a\,K_c} = 14_{3\,11}-13_{4\,10}$) in the ground state of DME at 68.7 GHz. At frequencies below 100 GHz, the torsional splitting is fully resolved for a large number of transitions. The spin statistical weights, denoted below each peak, closely match the observed intensity ratios.

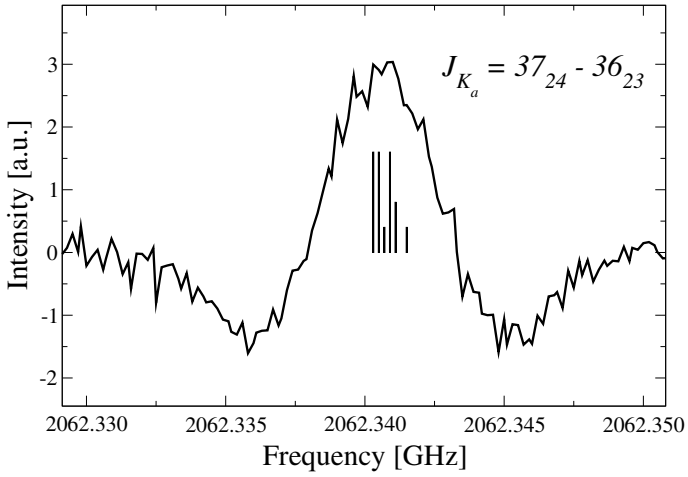

Fig. 5. Rotational transition ($J_{K_a} = 37_{24}-36_{23}$) in the ground state of DME at 2.06 THz. The spectrum recorded by the use of the 9th harmonic generated by a superlattice frequency multiplier (Endres et al. 2007) shows a typical line at frequencies around 2 THz. At these frequencies the torsional splitting usually remains unresolved due to the Doppler width.

are well represented in this spectral recording. These transitions provide valuable information, in particular for the accurate determination of the torsional splitting in energy levels with higher J and K values, because at high frequencies, the transitions involving these energy levels are usually blended due to the Doppler width. The signal-to-noise ratio allowed us to determine even very weak lines and a reasonable number of P-branch as well as $\Delta K = 3$ transitions were recorded. The already huge dataset in the *mm*-wavelength region reported in the literature was supplemented by several weaker lines and some of the reported frequencies were remeasured if they deviated widely from their predicted frequencies. The majority of recorded transitions were assigned at frequencies between 500 and 1000 GHz. In particular, Q-branch transitions including energy levels with high J quantum numbers up to 70 and fairly high K_a values up to 16 have been added. Broad scans have been performed in order to cover large frequency regions. Weaker transitions, in particular at high J values up to $J = 70$, have been recorded by the use of the BWO THz spectrometer. The density of spectral lines complicates the detection and the unambiguous assignment of a variety of weaker transitions including higher J quantum numbers, which hampered more extensive assignments. Mainly relatively strong R-branch transitions were accessed at frequencies above 1 THz involving energy levels with higher K_a values up to $K_a = 27$ at around 2 THz. The splitting was usually too small to be even partly resolved in the Doppler-limited measurements in this frequency domain. Figure 5 shows a typical transition above 2 THz.

The line assignments were relatively straightforward because of the quite large dataset. Using predictions based on this dataset, transitions in the spectra could be assigned step by step by improving frequency predictions iteratively. The main source of confusion is crossings which complicated the line assignments, as the usual labeling scheme based on the pseudo-quantum numbers K_a, K_c can provoke a change of the quantum numbers of levels in the vicinity of the level crossing if parameters change slightly. The asymmetry components are shifted differently by the internal rotation, which can lead to level crossings (Fig. 6), as has been discussed in Groner et al. (1998). Both asymmetry components of the EA and the EE states have the same symmetry in the G_{36} group. As a consequence, asymmetry levels mix if the size of the asymmetry

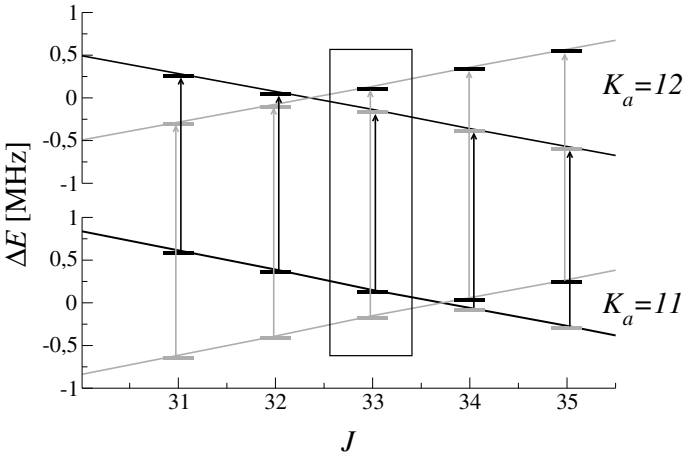

Fig. 6. Crossing of the energy levels of the substate EE for $K_a = 11$ and $K_a = 12$ due to the torsional splitting. The gray and black colored bars indicate energy levels with $K_c = J-K_a+1$ and $K_c = J-K_a$, respectively. ΔE is the energy difference between the energy of the corresponding asymmetry component and the averaged energy of both components. The arrows denote Q-branch transitions. The solid lines connect energy levels which belong to the same asymmetry component in dependence of J. Due to the crossing and the usual labeling scheme, the quantum numbers of the asymmetry components are interchanged (for $J = 35$ the black bars are located on the gray line and vice versa). The crossing is situated at different J values if K_a changes. Thus, c-type selection rules are obtained in the vicinity of the level crossings. In this example such a case, emphasized by the surrounding box, occurs at $J = 33$.

splitting decreases.The mixing affects predominantly transitions obeying b- and c-type selection rules of an ordinary asymmetric top molecule. On the other hand, the asymmetry components cannot be distinguished by the symmetry and the usual labeling by the pseudo-quantum numbers may fail and lead to c-type instead of b-type selection rules.

All lines were included in the analysis, including all previously reported ones. No blended lines were excluded, in contrast to the work of Groner et al. (1998), provided that the line profile could be sufficiently well reproduced. An overview of the lines used in the fit is given in Table 1. In cases where the same transition was reported in different papers, the frequency that fitted best was used in the fit. All other previously reported transitions were treated with their reported uncertainties, except transitions recorded with the $FASSST$ spectrometer. Based on our analysis, we suppose that the accuracy is slightly worse than 100 kHz on average. An accuracy of 150 kHz is used in our analysis instead. The dataset contains a large number of blended lines. In the least-squares fit, the intensity weighted frequency averages of the components of these blended transitions were used. The intensities were taken from predictions. Although systematic fitting problems associated with improper intensity predictions cannot be excluded and could lead to an incorrect description of the splitting, the matching of simulated and measured spectra indicates no obvious problems. In particular, the measurements at low frequencies confirm the agreement, because most of the transitions are fully resolved at high accuracies for a wide range of J and K values up to 54 and 19. The agreement between both the experimental and calculated splitting is very good, as shown in Fig. 3 for Q-branch transitions with $K_a = 6-5$ and $K_c = J - K_a + 1$. The solid lines connect calculated frequencies belonging to one of the four substates AA, EE, AE, and EA. The experimental values fit nicely within the given errors.

The analysis was performed using the computer programs ERHAM (Groner 1997) and SPFIT (Pickett 1991). ERHAM is based on the Hamiltonian given above. In Pickett's program SPFIT a similar Hamiltonian is used, which is also based on Fourier expansion series of the rotational constants and the energy terms. A detailed discussion of the different treatment in SPFIT compared to ERHAM has been given in the work of Drouin et al. (2006) on propane. In the present fit, an asymmetric rotor Hamiltonian in Watson's A reduction has been used. In total, 6830 transitions have been fitted using 34 spectroscopic parameters. 21 parameters correspond to rotational and centrifugal distortion constants up to the eighth order. In addition to the internal rotation parameters ρ and β, one energy tunneling parameter, ϵ_{10}, and ten tunneling parameters associated with the rotational constants were determined. The values of all parameters including their uncertainties are given in Table 2. The experimental dataset could be fit with ERHAM to experimental precision and a reduced standard deviation of $\sigma_{red} = 0.99$ was obtained. 30 frequencies deviated more than $3\,\sigma$, but no line more than $4.3\,\sigma$. The reduced standard deviation is reported for each dataset used in the fit in Table 1. The fit with SPFIT is slightly worse and the same experimental dataset could only be fitted to $\sigma_{red} = 1.5$ with a comparable number of parameters. The σ_{red} can be further reduced to 1.1 by the extensive use of tunneling parameters. However, the parameters are so strongly correlated in that case that the result of the fit and generated predictions become questionable.

5. Conclusion

New laboratory spectra of DME have been recorded from 38 GHz up to almost 2.1 THz. The existing dataset of rotation-torsional transitions within the vibrational ground state has been greatly extended. Transitions involving energy levels up to $J = 70$ and $K = 30$ have been analyzed and fitted to an effective Hamiltonian to experimental uncertainty. The ERHAM-model performed sufficiently well to analyze rotational spectra of molecules with two internal rotors having a barrier height of approximately 900 cm^{-1}. The differences of the SPFIT- and the ERHAM-approaches appear in the description of the torsional splitting and are thus particularly apparent at low frequencies and higher J, K values. The pure rotational parameters (not including tunneling) are in good agreement. The neglect of the $Y_{K'K}(K_1, K_2)$ terms, which describe the projection of the ρ-axis system onto the principal axis system, causes a less precise result in the SPFIT treatment. Since the torsional splitting in the ground state of DME is comparatively small, differences will become more obvious in the treatment of excited torsional states. A more detailed discussion will therefore be given in a separate work on the torsionally excited states.

The present analysis provides accurate and considerably improved predictions for the ground state spectrum of DME up to 2.5 THz. Frequencies of strong transitions in the THz frequency region with K values larger than 10 are typically improved by the order of several MHz. For example, the transition $J_{K_a} = 14_{13}-13_{12}$ at 995625 MHz is shifted by around 6 MHz compared to predictions based on Groner (1997). The most intense transitions are found at 1 THz for rotational temperatures of 200 K, which is a typical temperature for molecules in hot cores. Rotational temperatures of 89 K (Schilke et al. 1997) and 360 K (Schilke et al. 2001) have been reported for the vibrational ground state of DME in Orion KL. For all transitions involving energy levels with $E = 1500\,cm^{-1}$ and quantum numbers up to $J = 65$, $K = 30$, the accuracy is expected to be better than 1 MHz. For astronomical applications for which

Table 2. Spectroscopic parameters for DME in the vibrational ground state.

Parameter[a]	This work	Groner et al. (1998)
ρ	0.217131(37)	0.21709(21)
β (deg)	9.117(17)	8.631(13)
A (MHz)	38788.18325(28)	38788.17932(71)
B (MHz)	10056.482389(77)	10056.48166(18)
C (MHz)	8886.829843(75)	8886.82907(19)
Δ_J (kHz)	9.085900(59)	9.08387(36)
Δ_{JK} (kHz)	−26.86387(64)	−26.8656(39)
Δ_K (kHz)	341.9520(17)	341.721(41)
δ_J (kHz)	1.775148(25)	1.775099(53)
δ_K (kHz)	−13.8034(12)	−13.7825(44)
Φ_J (Hz)	0.007798(12)	0.00703(19)
Φ_{JK} (Hz)	0.1122(28)	0.1121(67)
Φ_{KJ} (Hz)	−4.0865(90)	−3.847(88)
Φ_K (Hz)	13.7300(72)	8.38(107)
ϕ_J (Hz)	0.003796(16)	0.003745(43)
ϕ_{JK} (Hz)	0.31571(57)	0.3341(57)
ϕ_K (Hz)	1.010(91)	1.50(22)
L_{JJK} (mHz)	0.00687(95)	
L_{JK} (mHz)	0.3079(35)	
L_{JKK} (mHz)	−0.7941(54)	
l_J (mHz)	0.0000260(30)	
l_{JKK} (mHz)	0.290(31)	
l_K (mHz)	6.671(37)	
Tunneling parameters[b]		
ϵ_{10} (MHz)	−3.0445(11)	−3.0435(41)
ϵ_{20} (MHz)		0.0053(16)
$[A-(B+C)/2]_{10}$ (kHz)	2.149(36)	1.64(21)
$[(B+C)/2]_{10}$ (kHz)	−0.416(11)	−0.0364(63)
$[(B-C)/4]_{10}$ (kHz)	−0.0908(92)	0.1116(37)
$[\Delta_J]_{10}$ (Hz)	0.2209(48)	
$[\Delta_{JK}]_{10}$ (Hz)	−1.797(36)	
$[\Delta_K]_{10}$ (Hz)	1.74(16)	
$[\delta_J]_{10}$ (Hz)	0.1579(82)	
$[\delta_K]_{10}$ (Hz)	1.099(64)	
$[\phi_J]_{10}$ (mHz)	−0.0432(16)	
$[\phi_K]_{10}$ (mHz)	−2.29(22)	

[a] The non-tunneling parameters $T_l^{(\kappa)}{}_{00}$ are labeled using the common notation for rotational constants.
[b] For tunneling parameters the notation $[\quad]_{qq'}$ has been used with the commonly used notation of corresponding non-tunneling parameters enclosed by the brackets.

1 MHz accuracy is usually sufficient, these predictions should give a reliable basis even for future observations with the new generation of telescopes. The quality of predictions is in particular sufficient to eliminate ground state transitions of DME as a source of line confusion. Above 1 THz the data fulfills the requirements needed in order to analyze future spectra recorded with the Herschel Space Observatory. The HIFI receiver aboard Herschel will give access to frequencies up to 1.91 THz with a spectral resolution better than 1.1 MHz. Also, the demand for precise frequency predictions of weaker transitions due to the improvement in sensitivity and spatial resolution granted by the Atacama Large Millimeter/submillimeter Array (ALMA) should be satisfied by the data of the present work. However, excited torsional states of DME will be sufficiently populated in hot core regions, such that the rotational transitions within these excited states will hamper the analysis of future spectra recorded by ALMA. An analysis of the two lowest excited torsional states is underway to provide extensive and accurate predictions over a large frequency range. All experimental frequencies included in our fit are given in Table A.1, available only at the CDS. The table shows the line assignments, the observed frequencies with the experimental uncertainties, the observed-calculated values, and a reference to the experimental work. They are also available through the Cologne Database for Molecular Spectroscopy (CDMS: http://www.cdms.de) (Müller et al. 2005, 2001) as well as through the JPL database (http://spec.jpl.nasa.gov) (Pickett et al. 1998) along with the predicted frequencies. The parameter files for both fitting routines (ERHAM and SPFIT) can be found in the example section of these databases.

Acknowledgements. The authors would like to thank P. Groner for his kind support and for valuable discussions. Funding has been provided by the Deutsche Forschungsgemeinschaft (DFG), in Cologne within the Sonderforschungsbereich (SFB) 494 and the Laboratoire Européen Associé (LEA) *HiRes*, administered by the DFG via Grant GI 319/1-1. H.S.P.M. has been supported by the Bundesministerium für Bildung und Forschung (BMBF) administered through Deutsches Zentrum für Luft- und Raumfahrt (DLR). Portions of this paper present research carried out at the Jet Propulsion Laboratory, California Institute of Technology, under contract with the National Aeronautics and Space Administration.

References

Blukis, U., Myers, R. J., & Kasai, P. H. 1963, J. Chem. Phys., 38, 2753
Drouin, B. J., Maiwald, F. W., & Pearson, J. C. 2005, Rev. Sci. Instr., 76, 093113
Drouin, B. J., Pearson, J. C., Walters, A., & Lattanzi, V. 2006, J. Mol. Spectrosc., 240, 227
Durig, J. R., Li, Y. S., & Groner, P. 1976, J. Mol. Spectrosc., 62, 159
Endres, C. P., Lewen, F., Giesen, T. F., et al. 2007, Rev. Sci. Instr., 78, 043106
Garrod, R., & Herbst, E. 2006, A&A, 457, 927
Garrod, R. T., Weaver, S. L. W., & Herbst, E. 2008, ApJ, 682, 283
Groner, P. 1997, J. Chem. Phys., 107, 4483
Groner, P., Albert, S., Herbst, E., & De Lucia, F. C. 1998, ApJ, 500, 1059
Lewen, F., Gendriesch, R., Pak, I., et al. 1998, Rev. Sci. Instr., 69, 32
Lovas, F. J., Lutz, H., & Dreizler, H. 1979, J. Phys. Chem. Ref. Data, 8, 1051
Müller, H. S. P., Thorwirth, S., Roth, D. A., & Winnewisser, G. 2001, A&A, 370, L49
Müller, H. S. P., Schlöder, F., Stutzki, J., & Winnewisser, G. 2005, J. Mol. Struct., 742, 215
Myers, R. J., & Wilson, E. B. 1960, J. Chem. Phys., 33, 186
Neustock, W., Guarnieri, A., Demaison, J., & Wlodarczak, G. 1990, Z. Naturforsch. A: Phys. Sci., 45, 702
Niide, Y., & Hayashi, M. 2003, J. Mol. Spectrosc., 220, 65
Pickett, H. M. 1991, J. Mol. Spectrosc., 148, 371
Pickett, H. M., Poynter, R. L., Cohen, E. A., et al. 1998, J. Quant. Spec. Radiat. Transf., 60, 883
Schilke, P., Groesbeck, T., Blake, G., & Phillips, T. 1997, ApJS, 108, 301
Schilke, P., Benford, D. J., Hunter, T. R., Lis, D. C., & Phillips, T. G. 2001, ApJS, 132, 281
Snyder, L. E., Buhl, D., Schwartz, P. R., et al. 1974, ApJ, 191, L79